REF: 607
Pa:2 **Pl: 2**

Measurement of the Photon Structure Function at $< Q^2 >$ of 279 GeV^2

The ALEPH Collaboration

Abstract

Inclusive $\gamma^*\gamma$ interactions to hadronic final states have been studied in the ALEPH data (taken from 1991 to 1995) where one scattered electron or positron is detected in the electromagnetic calorimeters. The event sample has been used to measure the hadronic photon structure function, F_2^γ at high Q^2. In addition, comparisons are made between the distributions measured in the data and those predicted from various simulations.

Submitted to the 1997 EPS-HEP Conference, Jerusalem

1 Introduction

In this paper measurements are presented of the hadronic structure function, F_2^γ, at high Q^2. In addition the data are compared to several different Monte Carlo generators for $\gamma^*\gamma$ collisions to test these generators at high Q^2.

The cross section for electron-positron scattering to produce hadrons by the exchange of two virtual photons is given in terms of the hadronic structure functions F_2^γ and F_L^γ by:

$$\frac{\mathrm{d}^3\sigma}{\mathrm{d}y\mathrm{d}x\mathrm{d}Q^2} = \frac{4\pi\alpha^2}{Q^4 x}\left(1-y+\frac{y^2}{2}\right)\left[F_2^\gamma(x,Q^2) - \frac{y^2}{2(1-y+\frac{y^2}{2})}F_L^\gamma(x,Q^2)\right]\Phi(x,y). \quad (1)$$

Here Q^2 is the four-momentum transferred to one of the virtual photons and is given by

$$Q^2 = 2EE'(1-cos\theta) \quad (2)$$

where E is the energy of the incident beam, E' and θ are the energy and scattering angle of the scattered electron, respectively. The Bjorken variable x is equal to the fraction of the momentum of the target photon carried by the struck quark in the Breit Frame and is given by

$$x = \frac{Q^2}{2pq} = \frac{Q^2}{(Q^2+W^2)} \quad (3)$$

where p and q are the 4 momenta of the two virtual photons and W is the total energy in the $\gamma^*\gamma$ centre of mass frame. The Bjorken variable y is given by

$$y = \frac{qp}{kp} = 1 - \frac{E'}{2E}(1+cos\theta) \quad (4)$$

where k is the four-momentum of the incident electron or positron which scatters with high Q^2. The function $\Phi(x,y)$ is the flux of the target virtual photons radiated from the other incident electron or positron and is given by [1]

$$\Phi = \frac{\alpha}{y\pi}\left[\left(1-\frac{Q^2}{\mathcal{X}}+\frac{Q^4}{2\mathcal{X}^2}\right) ln\frac{P^2_{max}}{P^2_{min}} - \frac{m_e^2 Q^4}{\mathcal{X}^2}\left(\frac{1}{P^2_{min}}-\frac{1}{P^2_{max}}\right)\right] \quad (5)$$

where

$$\mathcal{X} = 4E^2xy \quad (6)$$

and P^2_{min} and P^2_{max} are the minimum and maximum allowed values of the four-momentum transferred to the target virtual photons and m_e is the mass of the electron.

As the contribution from F_L^γ is expected to be small only F_2^γ is measurable in practice. The QCD description of F_2^γ divides into a perturbatively calculable 'point-like' part, and a non-perturbative 'hadronic' part. Several different authors [2, 3, 4, 5, 6] have attempted to calculate F_2^γ. Differences in their approach, particularly in handling the problems posed by the hadronic part, have led to a range of different predictions, particularly of the shape of the x distribution at low x. QCD predicts a logarithmic rise of F_2^γ with Q^2.

In this paper the hadronic structure functions are deduced from the measured rates of hadron production from $\gamma^*\gamma$ interactions using the above formulae. The data were selected so that the scattered electron 'tag' was detected in the main ALEPH electromagnetic calorimeters. Scattering at such large angles ensures that the photon radiated by the tag electron has a high Q^2. These data are therefore complementary to the lower Q^2 data published previously [10] in which the tag was detected in the small angle luminosity calorimeters.

2 Data Selection

This analysis uses the ALEPH data taken between 1991-1995 (luminosity 162 pb^{-1}). The number of high Q^2 $\gamma^*\gamma$ collisions expected in this sample is a few hundred, compared to the 4 million Z decays detected in the same period. The purpose of the data selection procedure is to extract a clean sample of $\gamma^*\gamma$ scattering events free from background due to Z decays.

The ALEPH detector has been described in detail elsewhere [7, 8]. The key components for observing the final state are the large time projection chamber (TPC) the electromagnetic calorimeter (ECAL) and the hadron calorimeter (HCAL). The two luminosity calorimeters LCAL and SICAL were used to measure the hadronic energy at small angles. The Inner Tracking Chamber (ITC) while primarily designed to supply fast track triggers, provides additional measurement of charged tracks. The muon chambers, the outermost part of the detector, were used for muon identification. The combination of dE/dx information from the TPC and the distribution of energy deposition in the calorimeters allows good identification of high energy electrons in the ALEPH detector [8].

The following cuts were applied to select a pure sample of $\gamma^*\gamma$ events. A tag was defined to be an identified electron with energy greater than 12 GeV, a scattering angle whose cosine was less than 0.955, and Q^2 less than 2400 GeV^2. A cone was constructed around the electron defined by an angle cosine greater than 0.995. Any identified photons within this cone were added to the electron four momentum to form the final 'tag'. The following cuts were then applied to eliminate background events from Z decays. Firstly to eliminate the bulk of $Z \to f^+f^-$ events,

- The number of tracks must be greater than 4 and less than 18.
- The Normalised Longitudinal Momenum Balance (NLMB) must be greater than 0.5 (NLMB=$cos\theta\Sigma p_z/|cos\theta|\Sigma E$).
- There must be no charged track or photon closer than 20 degrees to the tag.

Specific cuts against $Z \to \mu^+\mu^-, e^+e^-$ were then applied:

- The total electromagnetic energy must be less than 50 GeV .
- If the number of charged tracks is less than 7 then there must be no photon conversion to a positron electron pair nor more than one identified lepton of momentum greater than 6 GeV/c.

Background process	Events Surviving Cuts	Luminosity (pb^{-1})	Background (%)
$Z \to \mu^+\mu^-$	0	182	<1%
$Z \to ee$	0	108	<2%
$Z \to \tau^+\tau^-$	2	199	$\sim 1\%$
$Z \to qq$	4	71	$\sim 5\%$
$\gamma^*\gamma \to \tau^+\tau^-$ (tagged)	58	926	5.2±0.7%
$\gamma^*\gamma \to \tau^+\tau^-$ (untagged)	0	323	<0.5%

Table 1: Background Physics Processes calculated using Monte Carlo simulations

To eliminate $Z \to \tau^+\tau^-$:

- The total invariant mass of the observed hadrons, W_{vis}, must be greater than 2 GeV/c^2
- There must be at least one track or photon whose angle with respect to the tag had a cosine > -0.9

The total number of surviving events in the data was 193. The data covered the ranges $0 < x < 0.975$, $0 < y < 0.8$ and $50 < Q^2 < 2400$ GeV^2 with a mean value of Q^2 of 279 GeV^2. Table 1 shows the calculated number of background events from each physics source remaining after the cuts.

As the detection efficiencies are similar for high energy electrons and muons in the regions covered by this analysis [8] a direct measurement of the background in the data due to Z decay is possible. The data selection was repeated with the tag electron replaced by an identified muon. This resulted in a sample of 14 events. The data sample therefore consists of 179 genuine $\gamma^*\gamma$ events with a background of 7.8±2.1% events from Z decays. The background measured in this way is compatible with that determined from the simulations of Z decays (Table 1), so the muon events were used to correct for the background from Z decays by subtracting them bin by bin from all distributions.

The background of 5.2% (Table 1) from the process $\gamma^*\gamma \to \tau^+\tau^-$ where the scattered lepton was detected (tagged) was subtracted using simulated events. The beam-gas background was measured from the distribution of the vertex position along the beam direction to be less than 1% and was neglected.

W_{vis} and x_{vis} are defined as the values of W and x reconstructed from the observed hadronic final state particles. In order to minimise the amount of energy lost from each event the hadronic final state was reconstructed from all the measured hadronic energy in an event. In addition to the tracks and photons used in the event selection, this included the energy flow objects [9] in the luminosity calorimeters and clusters in the main calorimeters attributed to neutral hadrons. Small angle tracks with more than 4 ITC hits and momentum greater than 0.2 GeV/c were also included.

QPM program author	Hadronization Scheme	Mnemonic
Vermasseren	String only	PHO2NG
	Parton Shower + String	PHO2G
Berends, Darveveldt and Kleiss	String only	BDKNG
	Parton Shower + String	BDKG

Table 2: Summary of the QPM+VDM models used in this analysis.

3 Comparison with Models

To extract a measurement of the photon structure function from these data requires a reliable model of the production of hadronic final states by $\gamma\gamma$ collisions. There is at present no complete theoretical description of this process, so somewhat *ad hoc* models have to be used. Comparisons between such models and the data give some insight into the underlying physics.

The conventional approach to modelling the production of hadrons in $\gamma^*\gamma$ interactions is to combine models based on the Quark Parton Model, 'QPM', and the Vector Meson Dominance Model,'VDM'. Recently it has also become possible to use standard generators such as HERWIG. Both approaches have been employed in this analysis, using HERWIG 5.9 [16] for the latter.

For the VDM component of the conventional QPM+VDM approach the VDM model described in reference [14] was used in combination with two different implementations of the QPM. In addition, two alternative methods of hadronising the quarks were used for the QPM components, leading to a total of four different QPM+VDM models.

The hadronic part of the photon, simulated by the VDM model, is assumed to have a total cross section for $\gamma\gamma$ scattering of the form

$$\sigma_{\gamma\gamma} = \left(A + \frac{B}{W}\right) f(Q^2) \tag{7}$$

where A and B were taken to be 300 nb, and 300 nb GeV respectively. The Generalized VDM form factor [17], $f(Q^2)$, is given by

$$f(Q^2) = \Sigma R_i \frac{1 + Q^2/4M_i^2}{(1 + Q^2/M_i^2)^2} + \frac{0.22}{1 + Q^2/1.96} \tag{8}$$

where the summation is taken over three vector mesons of masses, M_i, equal to those of the ρ,ω and ϕ and the constants R_i were 0.65,0.08 and 0.05. In practice, the contribution from the term B/W was found to be negligible in this analysis and so it was not used.

One of the two QPM simulations used the program written by Vermaseren [15]. This is a lowest order QED calculation of the process $e^+e^- \to e^+e^-f\bar{f}$. It was used to produce events containing u,d or c quarks by setting the mass of the final state fermions to $m_u = 325, m_d = 325$ and $m_c = 1600\,\mathrm{Mev}/c^2$, respectively. The contribution of strange quarks is expected to be negligible and was neglected. The second QPM generator is the program of Berends, Darveveldt and Kleiss (BDK) [13], which includes processes in which photons are radiated from the incoming and outgoing electrons.

Model	VDM=0		VDM=1		QPM=1	
	QPM	VDM	QPM	VDM	QPM	VDM
PHO2G	1.78	0.0	1.46	1.0	1.0	2.22
PHO2NG	1.80	0.0	1.48	1.0	1.0	2.28
BDKG	1.49	0.0	1.22	1.0	1.0	1.63
BDKNG	1.78	0.0	1.46	1.0	1.0	2.28

Table 3: Weights obtained from the fit of models to the data.

The hadronization process was handled in all cases by the JETSET program [18]. Two alternative schemes were adopted; in one approach the quarks were passed directly to the string fragmentation procedure, while in the other the quarks were first allowed to radiate gluons via the parton shower scheme. In this case, Q^2_{max}, the maximum scale for the shower was set to W, the invariant mass of the final state. The resulting partons were then passed to the string fragmentation program for production of the final state hadrons. For the remainder of this paper the four QPM+VDM models are known by the mnemonics given in Table 2.

Samples from each QPM model were combined with the VDM sample to form a single set, weighting each sample so as to give the best overall value of χ^2 between the distributions predicted by the combined simulation and the data. Table 3 shows the relative proportions of the combined samples obtained by following this procedure. The values given in the table are the ratios of the measured to the expected weights which were calculated from the ratio of the experimental luminosity (162 pb^{-1}) to the luminosity of the simulations. For the HERWIG model an overall normalisation factor of 0.9 was found to give the best fit to the data. The histograms most sensitive to the mix of the models were the distributions of the tag energy, track multiplicities, track momenta and p_t, photon multiplicity, photon energy and p_t and total neutral energy. The pseudorapidity was also compared but never used since it gave a poor χ^2 value for all the models. Pseudorapidity is defined as $-\ln(\tan(\theta'/2))$ where θ' is the angle of an energy flow object with respect to the beam that has radiated the target photon.

The columns of Table 3 represent three extremes. One in which the VDM is given zero weight (VDM=0), one in which the VDM weight is held at its expected value (VDM=1) and one in which the QPM weight is held at its expected value (QPM=1). The choice of 'VDM=1' gives a fit to the data which is close to the minimum χ^2 point for all the distributions. The positions of the minima were consistent within their statistical errors for all the distributions used. The mean weighting factors for the two extremes were each two standard deviations away from that for 'VDM=1'. The use of these two extremes is thus a conservative choice when calculating the systematic error due to the fitting process.

Table 4 shows the values of χ^2 obtained when comparing each model to the data using the fit obtained with the 'VDM=1' weighting. A comparison between various distributions in the data and the models using these weighting factors is shown in Figure 1.

The BDKG model gave the most satisfactory χ^2 values in all the distributions used in the fit. For the simulations which only employed string fragmentation, PHO2NG and

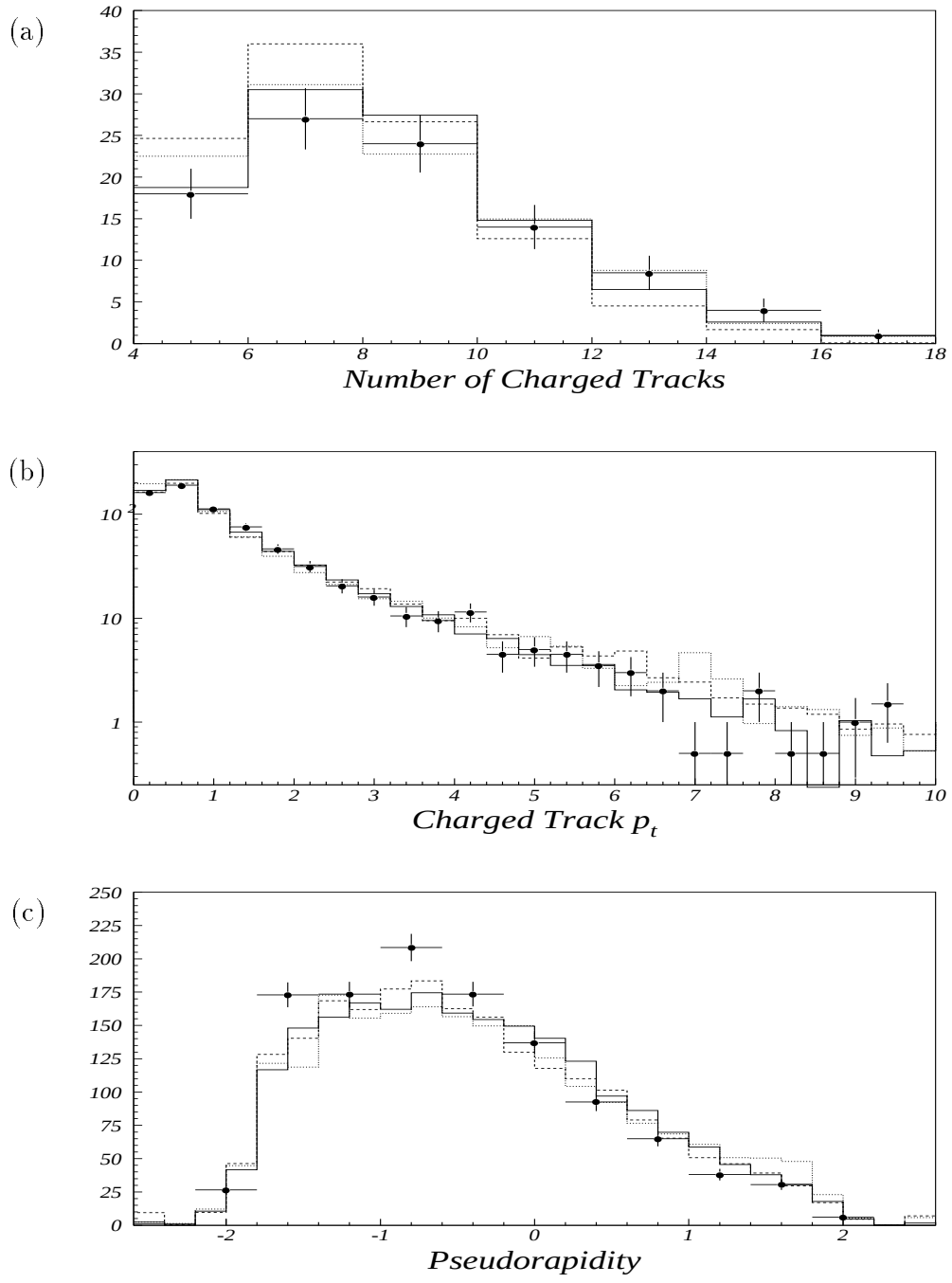

Figure 1: (a) Charged track multiplicity, (b) Transverse momentum of charged tracks, (c) Pseudorapidity of all charged tracks and neutral calorimeter objects. Histograms are the predictions of three of the models. The solid line is that of the BDKG simulation (parton showering enabled). The dashed line is for the PH02NG model (string fragmentation only). The dotted line is the result from the HERWIG program.

Distribution	PH02G	PHO2NG	BDKG	BDKNG	HERWIG
	χ^2 per data point				
E′	30.2/16	23.8/15	18.9/16	22.5/15	22.4/16
Track multiplicity.	9.5/10	21.3/9	9.2/10	17.3/9	11.8/10
Track momentum	16.6/23	18.9/24	13.5/21	20.0/24	33/24
Track p_t	18.8/27	32.4/30	22.1/26	39.4/31	59/30
γ multiplicity	4.2/7	6.7/7	8.3/8	14.7/7	13.7/7
γ energy	16.2/18	24.3/19	10.2/17	28.0/19	46/18
γ p_t	22.8/15	16.1/15	18.0/15	19.7/14	28/14
Neutral energy	13.6/7	11.1/7	13.4/6	19.3/8	11/7
Pseudorapidity	74/23	81/29	81/22	67/24	134/25

Table 4: χ^2 per data point between models and data

BDKNG, it was difficult to reconcile the track and photon multiplicities and their p_t distributions. This gives some evidence that gluon emission is a necessary ingredient of the models. The HERWIG model gave a poor representation of both the track and γ transverse momentum spectra. All the χ^2 values seem to be somewhat better than those found at lower values of Q^2 [12].

It can be seen from Table 4 and Figure 1(c) that none of the models gives an acceptable representation of the pseudorapidity distribution. The models all predict too much hadronic activity at positive pseudorapidity with too little at negative values. This is consistent with the observation reported by OPAL [19]. Large discrepancies are also observed in this variable in the ALEPH and OPAL data at lower Q^2 [10, 12, 19], but in that case the data exceeds the models at positive values of pseudorapidity.

The reconstruction of events is incomplete due to the lack of coverage of the detector for the hadronic final state, principally in the region close to the beam pipe. This is illustrated in Figure 2 (a) which shows x_{vis}, the reconstructed value of x, plotted as a function of the true value of x for events generated using the BDKG model. The effects of the energy losses can be clearly seen in the tendency for x_{vis} to be greater than the true values of x.

The reconstruction of Q^2 is more accurate than that of x, however some smearing does occur. Figure 2 (b) shows the reconstructed value of Q^2 as a function of the generated values for the QPM component of the BDKG model. Part of the smearing is due to the experimental resolution and part is due to initial and final state radiation. The trend for the measured value of Q^2 to be less than the true value is due mainly to initial state radiation along the electron or positron line which provided the high Q^2 photon. The effects of final state radiation are minimised by the merging of close photons with the tag described in section 2.

The radiative effects in this kinematic region are predicted to be relatively large compared to those at lower Q^2 [20]. However the results from the BDK model in which radiative effects are taken care of, and the others, in which they are ignored, do not differ significantly compared to the statistical errors on the data. Hence radiative effects are

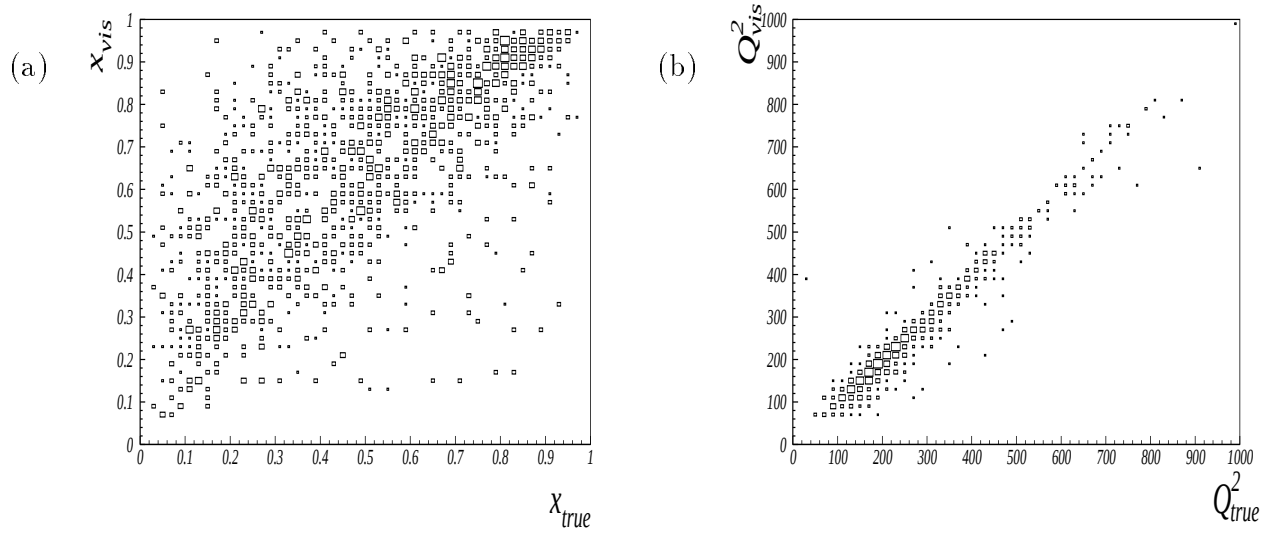

Figure 2: (a) The reconstructed value of x versus the true value for the sum of QPM and VDM models. (b) The reconstructed value of Q^2 versus the true value from the Behrends Darverveldt and Kleiss QPM simulation.

relatively insignificant in this analysis.

4 Comparison of the Data with Structure Function Parameterisations

There are a number of parameterisations of the structure function F_2^γ [3, 4, 5, 6] which can be compared with the data. In order to do this the parameterisations have to be folded with the various terms in equation 1 and the detector response measured from the simulations. The number of events in any experimental bin, N, is given by

$$N = \int\int\int G(x,y,Q^2)\mathcal{F}(x,Q^2)P(x,x_{vis},y,y_{vis},Q^2,Q^2_{vis})\epsilon(x,y,Q^2)\mathrm{d}x\mathrm{d}y\mathrm{d}Q^2 \qquad (9)$$

where $\mathcal{F}(x,Q^2)$ is defined as

$$\mathcal{F}(x,Q^2) = \left[F_2^\gamma(x,Q^2) - \frac{y^2}{2(1-y+\frac{y^2}{2})}F_L^\gamma(x,Q^2)\right], \qquad (10)$$

$G(x,y,Q^2)$ absorbs all the remaining QED factors in equation 1

$$G(x,y,Q^2) = \frac{4\pi\alpha^2}{Q^4 x}\left(1-y+\frac{y^2}{2}\right)\Phi(x,y) \qquad (11)$$

$P(x,x_{vis},y,y_{vis},Q^2,Q^2_{vis})$ are the probabilities that an event produced at x,y and Q^2 will be measured at x_{vis}, y_{vis} and Q^2_{vis}, respectively, and $\epsilon(x,y,Q^2)$ is the apparatus acceptance.

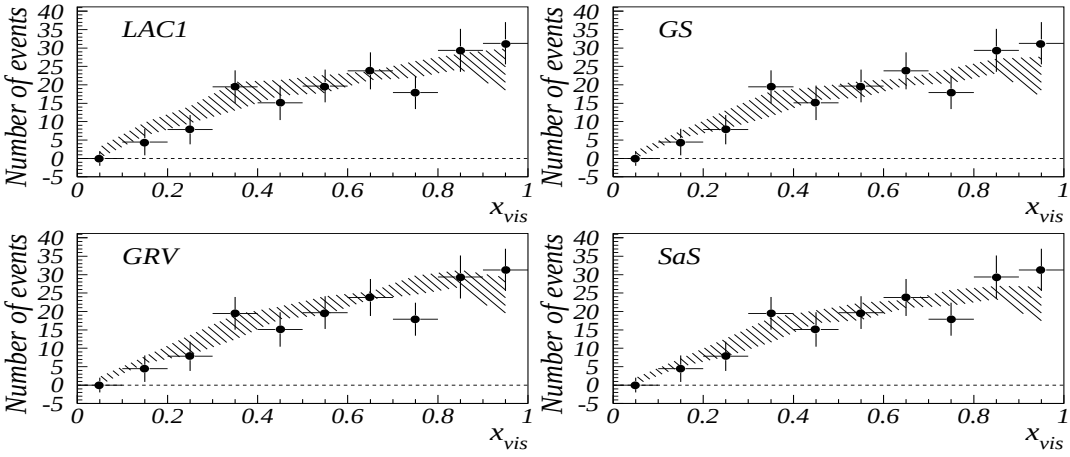

Figure 3: The measured values of x_{vis} compared to predictions from four different structure function parameterisations. The shaded areas show the spread of the predictions coming from the use of of the five different models used to compute the acceptance and smearing matrices.

$P(x, x_{vis}, y, y_{vis}, Q^2, Q^2_{vis})$ and $\epsilon(x, y, Q^2)$ are both measured from the simulations. The integral covers the range of the experimental bin under consideration.

Figure 3 shows the measured x_{vis} distribution. The shaded area shows the results obtained by using equation 9 to predict the x_{vis} distribution. The spread of the predicted values is due to the use of the five different sets of simulations to calculate the detector effects represented by $P(x, x_{vis}, y, y_{vis}, Q^2, Q^2_{vis})$ and $\epsilon(x, y, Q^2)$ and indicates the systematic error on the method due to variations in the modelling of the hadronic final state. The procedure was repeated with four different parameterisations of F_2^γ ; those of Gordon and Storrow (GS) [3], Glück, Reya and Vogt (GRV) [4], set I of Abramowicz, Charcula and Levy (LAC1) [5] and set 1D of Schuler and Sjöstrand, (SaS) [6]. In all cases the longitudinal structure function $F_L^\gamma(x, Q^2)$ was set to zero. There is good agreement between the data and the calculated distributions showing that the parameterisations of the structure functions all give an adequate representation of the data with no single parameterisation being preferred.

5 Extraction of the Structure Function F_2^γ

The structure functions F_2^γ can be obtained from a measurement of $\mathrm{d}\sigma/\mathrm{d}x$ (equation 1). This differential cross section is obtained from the x distribution of the data divided by the integrated luminosity of the experiment and the apparatus acceptance. Dividing the differential cross section by the integral of the function $G(x, y, Q^2)$ (equation 11) gives the function $\mathcal{F}(x, Q^2)$ (equation 10).

	$0 < x < 0.35$	$0.35 < x < 0.65$	$0.65 < x < 1$
F_2^γ/α	0.44	0.78	1.36
Statistical error	0.13	0.11	0.29
Model error	0.06	0.02	0.31
Fitting error	0.08	0.05	0.01
Total error	0.16	0.12	0.42

Table 5: The Structure Function F_2^γ/α in three x bins.

As x_{vis}, the measured value of x is smeared asymmetrically from the true value, an unfolding procedure is necessary to extract the true x distributions from the data. The unfolding was performed using the Blobel procedure[21] which fits a sum of spline curves to the data after passing them through the $x_{\rm vis}$ versus $x_{\rm true}$ matrix obtained from the simulated events. A regularisation procedure is used to suppress oscillations in the result which have higher frequency than are justified by the resolution of the input measurements. This gave the number of events in bins of x_{true} which was then used to obtain the differential cross section $\mathrm{d}\sigma/\mathrm{d}x$. This in turn was divided by the integrals of $G(x, y, Q^2)$, evaluated numerically, to obtain measurements of $\mathcal{F}$.

Making the standard assumption that the contribution of the hadronic longitudinal structure function, $F_L(x, Q^2)$, is negligible the measured function, $\mathcal{F}$, gives directly the hadronic photon structure function F_2^γ. The resulting measurements of F_2^γ are listed in Table 5 where each of the five simulations has been used in turn to find the smearing matrix and acceptance corrections. The final value of the structure function is obtained using the BDKG model as this gave the best representation of the data. The standard deviation of the results obtained using each of the five models with the optimum fit was used for the model systematic error. A systematic error due to the fitting procedure described in section 3 was obtained from the change in the structure functions as the VDM mix was varied between the extremes shown in Table 3 (VDM=0 and QPM=1) for the BDKG model. The remaining systematic errors are expected to be small compared with these systematic errors and the statistical errors.

Figure 4 shows the values of F_2^γ obtained in this way as a function of x. The statistical errors are given by the inner error bars and the outer error bars represent the total errors from adding the statistical and systematic errors in quadrature. Comparison is made with various parameterisations [4, 5, 6] which all give a good representation of the data. Figures 5(a) and (b) show comparisons with other measurements. There is good agreement between these and the data presented here.

6 Conclusions

Inclusive production of hadrons in $\gamma^*\gamma$ interactions at $< Q^2 >$ of 279 GeV^2 has been studied in the ALEPH data taken between 1991 to 1995. The hadronic final state is found to be best represented by a mixture of models based on the Vector Meson Dominance

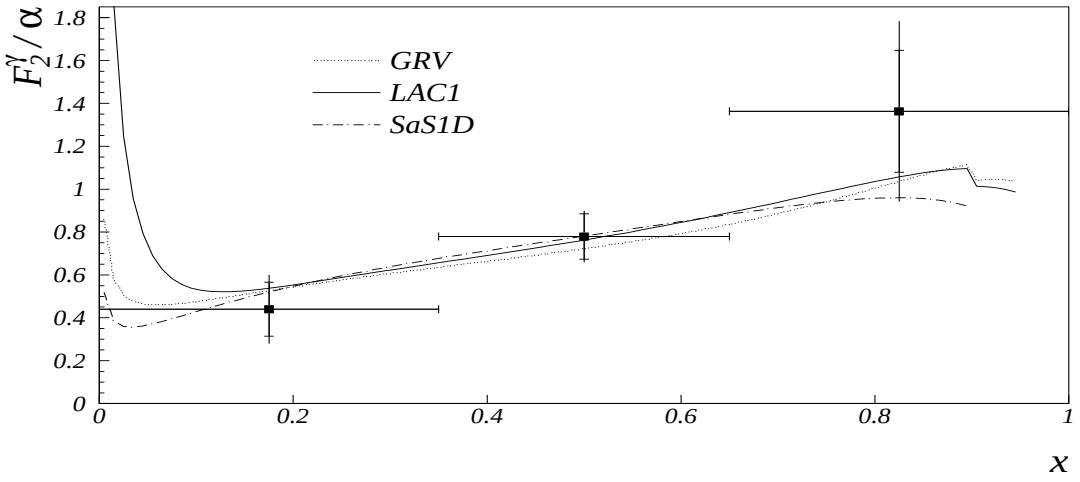

Figure 4: The values of F_2^γ as a function of x compared to three parameterisations.

model with a cross section of ∼300 nb and the QPM model of quark-antiquark pair production in $\gamma^*\gamma$ collisions of Berends, Darveveldt and Kleiss with the parton shower model included in the hadronization of the quarks.

The event sample has been used to measure the hadronic photon structure function, F_2^γ. The measurements of F_2^γ are found to be compatible with parameterisations of the parton distributions of the photon.

Acknowledgements

We would like to thank our colleagues of the accelerator divisions at CERN for the outstanding performance of the LEP machine. Thanks are also due to the many engineers, and technical personnel at CERN and at the home institutes for their contribution to ALEPH's success. Those of us not from member states wish to thank CERN for its hospitality.

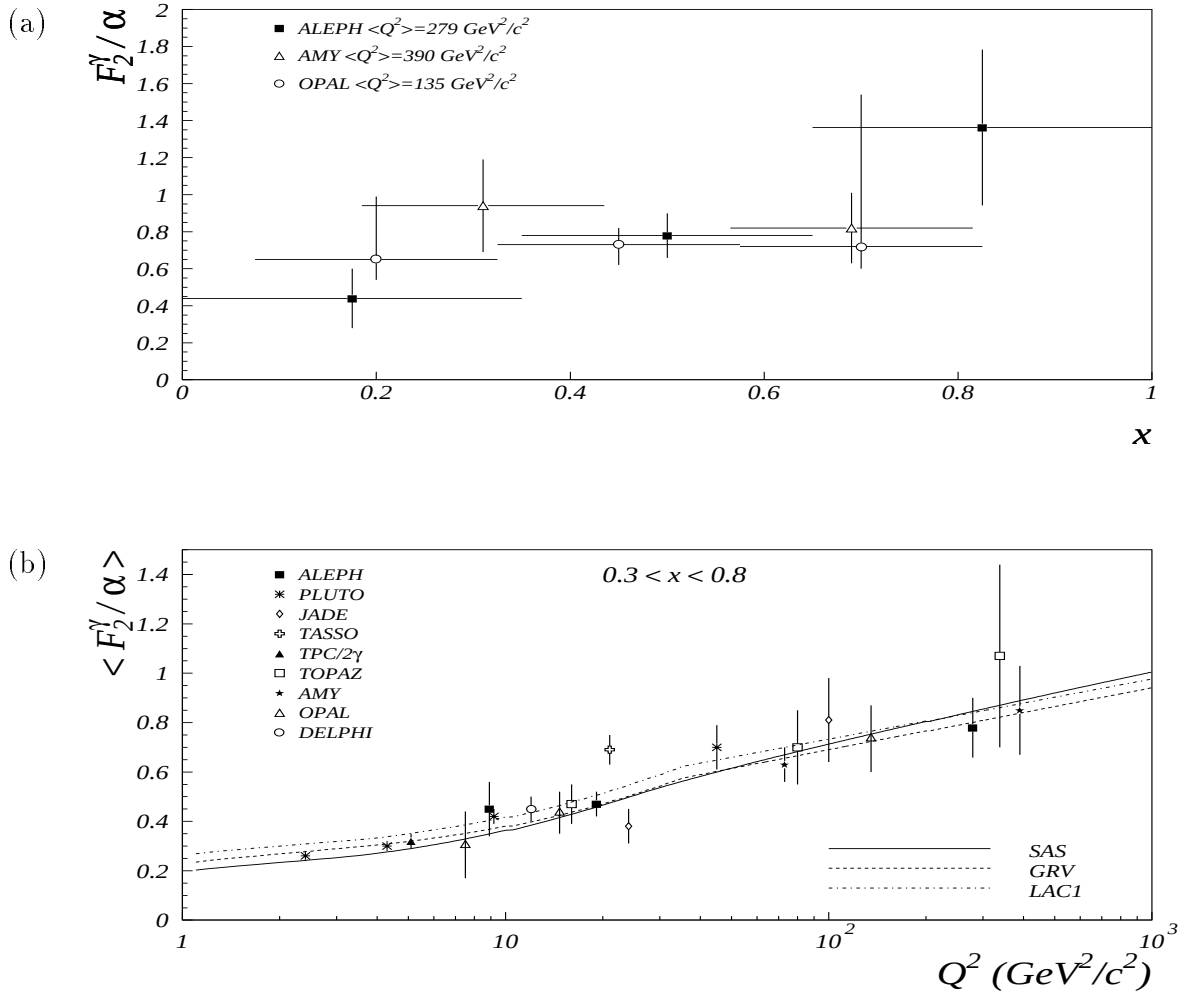

Figure 5: The values of F_2^γ measured in this experiment; (a) as a function of x and compared to other data at similar Q^2, and (b) averaged over the region $0.3 < x < 0.8$ and compared both to results from other experiments and to the values obtained from three parameterisations.

References

[1] Particle Data Table, Phys. Rev. **D54** (1996) page 180.

[2] M. Drees and R.M. Godbole, *J. Phys.* **G21** (1995) 1559.

[3] L.E. Gordon and J.K. Storrow, *Z. Phys.* **C56** (1992) 307.

[4] M. Glück, E. Reya and A. Vogt, *Phys. Rev.* **D45** (1992) 3986.

[5] H. Abramowicz, K. Charchula and A. Levy, *Phys. Lett.* **B269** (1991) 458.

[6] G. A. Schuler and T. Sjöstrand, *Z. Phys.* **C68** (1995) 607.

[7] ALEPH collab., D. Decamp et al., *Nucl. Instr. Meth.* **A 294** (1990) 121.

[8] ALEPH collab., D. Buskulic et al., *Nucl. Instr. Meth.* **A360** (1995) 481.

[9] ALEPH collab., D. Decamp et al., *Phys. Lett.* **B246** (1990) 306.

[10] A.J. Finch *Measurement of the Photon Structure Function* in Proceedings of Photon'97 (1997).

[11] JADE collab., W. Bartel et al., *Z. Phys.* **C24** (1984) 231.

[12] RAL-TH-97-005, A Measurement of the Photon Structure Function $F_2^\gamma(x, Q^2)$, Using the ALEPH Detector. Gordon R. Crawford University of Lancaster. PhD thesis, December 1996

[13] F.A. Berends, P.H. Daverveldt and R. Kleiss, Comp. Phys. Comm. **40** (1986) 285.

[14] ALEPH collab., D. Buskulic et al., *Phys. Lett.* **B313** (1993) 509.

[15] J.A.M. Vermaseren, in Proceedings of the IV International Workshop on Gamma Gamma Interactions, eds. G. Cochard and P. Kessler (1980);
Long program write up by J.A.M. Vermaseren (unpubl.).

[16] G. Marchesini, et al., *Computer Phys. Commun.* **67** (1992) 465.

[17] I.F. Ginzberg and V.G. Serbo, *Phys. Lett.* **B109** (1982) 231.

[18] T. Sjöstrand, *Computer Phys. Commun.* **82** (1994) 74.

[19] OPAL Collab., K. Ackerstaff et al., *Z. Phys.* **C74** (1997) 33.

[20] E. Laenen and G. Schuler, Phys.Lett. **B374** (1996) 217.

[21] V. Blobel in Proceedings of the CERN School of Computing, Aiguablava, Spain (1984), CERN 85-09.